EPJ E
Soft Matter
www.epj.org

Eur. Phys. J. E **27**, 171–184 (2008) DOI: 10.1140/epje/i2008-10367-6

Phase behaviour of a dispersion of charge-stabilised colloidal spheres with added non-adsorbing interacting polymer chains

C. Gögelein and R. Tuinier

EDP SCIENCES
Società Italiana Di Fisica
Springer

Eur. Phys. J. E **27**, 171–184 (2008)
DOI 10.1140/epje/i2008-10367-6

THE EUROPEAN PHYSICAL JOURNAL E

Phase behaviour of a dispersion of charge-stabilised colloidal spheres with added non-adsorbing interacting polymer chains

C. Gögelein[a] and R. Tuinier[b]

Institut für Festkörperforschung, Teilinstitut Weiche Materie, Forschungszentrum Jülich, D-52425 Jülich, Germany

Received 21 May 2008 and Received in final form 4 August 2008
Published online: 16 September 2008 –

Abstract. We present a theory for the phase behaviour of mixtures of charge-stabilised colloidal spheres plus interacting polymer chains in good and θ-solvents within the framework of free-volume theory. We use simple but accurate combination rules for the depletion thickness around a colloidal particle and for the osmotic pressure up to the semi-dilute concentration regime. Hence, we obtain expressions for the free energy for mixtures of charged colloidal particles and non-adsorbing interacting polymers. From that, we calculate the phase behaviour, and discuss its topology in dependence on the competition between the charge-induced repulsion and the polymer-induced attraction. The homogeneous mixture of colloids and polymers becomes more stabilised against demixing when increasing the electrostatic repulsion. This charge-induced stabilisation is strongest for small polymer-to-colloid size ratios and is more pronounced for charged colloids mixed with polymers in a good solvent than for polymers in a θ-solvent. For the weakly charged regime we find that the phase diagram becomes salt-concentration–independent in the protein limit for charged colloids plus polymers in a θ-solvent. The liquid window, *i.e.*, the concentration regimes where a colloidal liquid exists, is narrowed down upon increasing the charge-induced repulsion. Also this effect is more pronounced when charged colloids are mixed with polymer chains in a good solvent. In summary, we demonstrate that the solvent quality significantly influences the phase behaviour of mixtures of charged colloids plus non-adsorbing polymers if the range of the screened electrostatic repulsion becomes of the order of the range of the depletion-induced attraction.

PACS. 82.70.Dd Colloids – 61.25.H- Macromolecular and polymers solutions; polymer melts – 68.35.Rh Phase transitions and critical phenomena

1 Introduction

Adding non-adsorbing polymers to a dispersion of colloidal particles induces attractive forces between them [1–3]. These attractive interactions are due to the loss of conformational entropy if a polymer approaches a particle surface, leading to a polymer-depleted zone around the particle. Overlapping of two depletion zones causes an inhomogeneous pressure distribution by the dissolved polymers around the two neighbouring particles, and, thus, an attractive force between them. This depletion interaction has first been described by Asakura and Oosawa [4,5] (AO), and was later rediscovered by Vrij [6]. In Vrij's model for mixtures of polymers and colloids, the polymers are freely inter-penetrable (mimicking ideal chains), while there is a hard-sphere repulsion between the colloids and the polymers. This situation corresponds to hard spheres dispersed in a dilute polymer solution.

The first success in describing the experimentally observed phase behaviour of colloid-polymer mixtures semi-quantitatively has been made by Gast *et al.* [7] using thermodynamic perturbation theory (TPT). Gas-liquid and fluid-solid phase transitions have been predicted by TPT in accordance with experimental results. Gast *et al.* [7] also showed analytically that the assumption of a pairwise additive interaction potential in TPT is exact for polymer-to-colloid size ratios $q \leq 0.1547$, where $q = R_g/a$ with the polymer's radius of gyration R_g and the hard sphere radius a. For $q > 0.1547$ multiple overlap of depletion zones can occur and many-body interactions have to be taken into account. De Hek and Vrij [8] performed experiments on model hard-sphere–like systems with added non-adsorbing polymer chains using silica particles and polystyrene in cyclohexane. They observed separation into two coexisting fluid phases. The coexistence between a stable fluid and solid was observed for instance by Vincent *et al.* [9,10].

The partitioning of the polymers over the coexisting colloid-poor and colloid-rich phases has first been

[a] e-mail: c.goegelein@fz-juelich.de
[b] *Present address:* DSM Research, ACES, P.O. Box 18, 6160 MD Geleen, The Netherlands.

described by the free-volume theory (FVT) by Lekkerkerker *et al.* [11]. Here, the main step was to approximate the free-volume accessible to the freely overlapping polymer coils by using scaled particle theory (SPT) [12,13]. Meijer and Frenkel [14] used a lattice model for the mixture of hard spheres and polymers and Monte Carlo (MC) simulation techniques to investigate the accuracy of SPT and TPT. These theories use the AO model, where the deformability of the polymer coil is not taken into account. The simulation data show that polymer-induced many-body interactions have to be taken into account for $q > 0.2$. The theory of Lekkerkerker *et al.* [11] performs overall very well but leads to deviations around the gas-liquid critical point [15]. Dijkstra *et al.* [16–20] verified and extended the statistical-mechanical derivation of the thermodynamic properties of colloid-polymer mixtures by Meijer and Frenkel [14]. They observed good agreement for equal sizes of polymer and colloid comparing their computer simulation data using the effective one-component AO model with FVT [20]. Moncho-Jordá *et al.* [21] investigated the AO model for $q \gg 1$ (protein limit), where many-body interactions become important. Good agreement was found between the binodals predicted by FVT and the computer simulation data.

Fuchs, Schweizer, and co-workers [22–26] used an off-lattice Polymer Reference Interaction Site Model (PRISM) integral equation method with a modified Percus-Yevick closure to derive analytical expressions and compute numerical results for a mixture containing hard spheres and non-adsorbing polymer chains. Because calculating the binodal coexistence curves is extremely numerical demanding within PRISM, Zukoski and co-workers [27–29] have restricted themselves to compare theoretically predicted spinodal decomposition curves with binodals in mixtures of effectively hard-sphere–like silica particles and polystyrene polymer chains under θ- (decalin) and good (toluene) solvent conditions. Good agreement has been found which encourages further investigations using this approach. Compared to the free-volume approach yielding macroscopic thermodynamic quantities, the liquid-state theory derived by Fuchs and Schweizer gives quantitative predictions for the microscopic structure of colloid-polymer mixtures which can be verified by appropriate scattering studies. It will be interesting, for instance, to investigate Fuchs and Schweizer's predictions on long-ranged polymer-mediated attractive forces [26], which might be related to recent observations of critical phenomena in colloid-polymer mixtures [30,31].

The fundamental interest on the influence of the attractive polymer-induced depletion forces on colloidal dispersions focused especially on studying the global phase behaviour in dependence of the range of attraction through the polymer-to-colloid size ratio. Besides that, there is also a need to include properties of non-ideal polymer solutions plus non-hard-sphere colloids to describe industrial colloid-polymer dispersions. Concerning the colloids, a practical situation is to account for screened electrostatic charges on the colloidal particles from surface-released counter-ions (see Fig. 1). Apart from applications like paints or processed food [32,33], one encounters such systems for example in biology, and, especially, in the cell, where 20–30% of the volume is occupied by soluble proteins and other biomacromolecules [34]. Here, one expects that depletion interactions play a major role in the self-organisation of biomacromolecules, *e.g.*, the self-assembling of DNA [35] or the bundling of f-actin fibres [36]. The aim is therefore to find reasonably simple but accurate expressions to calculate the phase behaviour of charged spheres in a crowded (semi-dilute) (bio-)macromolecular (polymer) environment. An additional need to describe such mixtures of charged colloids and interacting polymers results from crystallography to determine the atomic structure of proteins. Here, polymers are often added to protein solutions at high salt concentration to accelerate crystallisation or to obtain regular crystals [37]. Not many attempts have been made to describe such systems.

Another approach to include the influence of non-ideal polymers has been made by approximating polymers as soft colloids [38–40], and quantitative agreement with computer simulation data on the phase behaviour of colloids and self-avoiding polymers has been found [41] on the level of the depletion interaction between two hard walls. A disadvantage of this approach is that it relies on Monte Carlo simulations as an input to adjust polymer-polymer and colloid-polymer interactions.

Schmidt and Fuchs [42] derived a penetrable Asakura-Oosawa model (PAO) using density functional theory. The model allows colloids to penetrate the polymer spheres by introducing a repulsive step-function colloid-polymer pair potential. The strength of the colloid-polymer repulsions is adjusted using known expressions from renormalisation group theory for the insertion energy of adding colloids into a dilute polymer solution at θ- and good-solvent conditions. Essentially, the model reduces to the functional AO model with a polymer-to-colloid size-ratio–dependent colloid packing fraction neglecting polymer-polymer interactions. The PAO model agrees well with results from the PRISM approach.

The influence of excluded-volume polymer chains on the phase behaviour of colloidal spheres has first been incorporated within the free-volume theory by Aarts *et al.* [43] using results from Renormalisation Group theory [44,45] for the correlation length in polymer solutions.

The phase equilibrium of charged colloidal particles with polymer-induced depletion interaction has been investigated by Tavares and Sandler [46] using TPT and Gibbs ensemble Monte Carlo simulations. In this work the electrostatic repulsion was modelled on a Debye-Hückel level and van der Waals interactions were included as well. They observed that the additional van der Waals attraction widens the fluid-solid coexistence curves and destabilises the dispersion against gas-liquid phase separation. On the other hand, the repulsive electrostatic forces tremendously stabilise the colloid-polymer mixture against phase separation. Thus, the fluid-solid coexistence curve shifts to higher polymer concentrations upon increasing the screened electrostatic repulsions.

Later on, Ferreira *et al.* [47] have calculated spinodal decomposition curves using liquid-state theory for charged colloids and neutral polymers *inter alia*. They also observed that the electrostatic repulsion between highly charged colloids [48] significantly stabilises mixtures of charged colloids and non-adsorbing polymers against gas-liquid phase separation (see Fig. 11 and discussion on p. 9860 in [47]).

Denton and Schmidt [49] included electrostatic repulsive forces due to screened charges in the free-volume theory. In their model, the electrostatic repulsions were mapped onto effective hard-sphere interactions and the additivity of the mixture was restored by scaling the radius of gyration of the polymer. Fortini *et al.* [50] proposed a similar way to include highly screened electrostatic Coulomb interactions to the free-volume theory by mapping the repulsive interactions onto effective hard-sphere ones. In their approach, the non-additivity of the mixture was not restored by (down-)scaling the polymer size. Instead, the free-volume fraction was reanalysed from SPT, and a semi-quantitatively accurate description was proposed, which describes their computer simulation data reasonably well. In contrast, the model by Denton and Schmidt underestimates the osmotic pressure of the polymer solution significantly. Thus, it follows that rescaling the polymers and ensuring an additive mixture is inappropriate in describing highly screened or, conversely, weakly charged colloidal dispersions containing non-adsorbing polymers.

Fleer and Tuinier [51] extended the free-volume approach for colloid-polymer mixtures up to and including the semi-dilute concentration regime for interacting polymer solutions using scaling arguments for the depletion thickness and osmotic pressure. Their expressions for the depletion thickness and osmotic pressure were tested against experimental and computer simulation data [52]. Quite recently, Tuinier *et al.* [53] have compared this approach to experimental data on the gas-liquid phase coexistence diagram of hard-sphere–like poly-methylmethacrylate colloids with added flexible polystyrene chains dispersed in cis-decalin and found excellent quantitative agreement. This improved free-volume theory was named generalised free-volume theory (GFVT). Based on this adequate refinement, we feel encouraged to apply the GFVT to mixtures of charged colloids and interacting polymer solutions.

In this work we present a generalised free-volume theory which predicts the equilibrium phase behaviour of mixtures of polymers and charge-stabilised colloidal spheres in either a θ- or good solvent. We calculated the fluid-solid and gas-liquid coexistence curves for various size ratios of the polymers and the colloids and for various screening lengths. Here, we restrict ourselves to the regime of weakly charged or, equivalently, highly screened particles, where the electrostatic pair interactions can be mapped accurately onto an effective hard-sphere interaction. We also discuss the influence of the solvent quality and the effect of the electrostatic repulsion on the stability of a homogeneous fluid phase with respect to a gas-liquid phase demixing and we further focus on the effect of salinity on the location of the critical end-point.

2 Model of weakly charged colloidal particles and non-adsorbing polymer chains

We now proceed to explain how we map the system of charged colloids onto effective hard-sphere ones. In Section 3, the polymers, which in addition insert depletion-induced attractive interactions to the system, are taken into account. As an application for our model calculations one might think of weakly charged sphere-like proteins at high salt content dispersed in a polymer solution to accelerate crystallisation. Thus, we assume that the electrostatic Coulomb interactions are highly screened, and, therefore, short-ranged. We also assume that correlation effects between the micro-ions (added salt and surface released counter-ions), which might arise due to the comparable size between the micro-ions and macro-ions (proteins), can be neglected. This assumption may even hold for high salt concentrations in case of monovalent co- and counter-ions. We describe the electrostatic repulsion by a Debye-Hückel screened Yukawa-like pair interaction potential

$$\beta u_{\rm cc}(r) = \begin{cases} \infty, & r \le 2a, \\ \dfrac{Z^2\, l_{\rm B}}{(1+\kappa a)^2}\, \dfrac{\exp[-\kappa(r-2a)]}{r}, & r > 2a, \end{cases} \tag{1}$$

where Z is the protein charge number and $l_{\rm B} = e^2/(4\pi\varepsilon_0\varepsilon\, k_{\rm B}T)$ is the Bjerrum length with the dielectric constant *in vacuo* ε_0, the dielectric solvent constant ε, and the elementary charge e. The colloidal particle radius is denoted by a. The square of the Debye screening parameter κ is given as

$$\kappa^2 = 4\pi l_{\rm B} \left(Z\rho_{\rm c} + \sum_s \rho_{\rm s} \right), \tag{2}$$

where $\rho_{\rm c}$ is the colloid number density. The first term between the brackets accounts for monovalent counter-ions released from the colloid surface, and the second for the additionally inserted monovalent micro-ions with number density $\rho_{\rm s}$. For later use we introduce the reduced contact value of the repulsive pair interaction potential as $\beta\epsilon = 2\, Z^2\, l_{\rm B}\, a/(1+\kappa a)^2$.

As discussed previously by Fortini *et al.* [50], one can map electrostatic repulsions onto effective hard-sphere interactions provided the colloidal net charges are sufficiently screened by the co- and counter-ions or provided that the colloidal particles are sufficiently weakly charged. The resulting effective volume fraction, $\eta_{\rm c}'$, is defined by

$$\eta_{\rm c}' = \left(\frac{a'}{a}\right)^3 \eta_{\rm c} = m\,\eta_{\rm c}, \tag{3}$$

where a' describes the effective colloidal radius, and $\eta_{\rm c} = 4\pi a^3\rho_{\rm c}/3$ denotes the colloid volume fraction. The factor m is defined as the cubed size ratio between the effective, a', and bare colloidal particle radius, a. The effective radius a' of a charged colloidal sphere is calculated using the

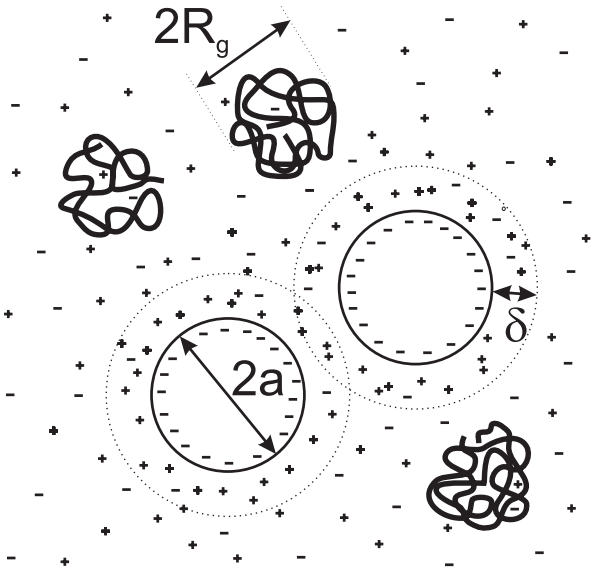

Fig. 1. Schematic drawing of two negatively charged colloidal particles with diameter $2a$ in a solution with neutral polymers with a radius of gyration R_g. The depletion zone with thickness δ is indicated by the dotted circles around the colloidal particles. The micro-ions are illustrated by little plus (+) and minus (−) signs. These micro-ions build up the electrostatic double layer around the charged colloidal particles. Because of the negatively charged macro-ions (colloids), the concentration of counter-ions (+) increases whereas the number of co-ions (−) decreases upon approaching the colloidal surface.

expression found by Barker and Henderson [54] from TPT

$$a' = a + \frac{1}{2}\int_{2a}^{\infty} \mathrm{d}r\,(1 - \exp[-\beta u_\mathrm{cc}(r)]). \qquad (4)$$

Now, after we have mapped the charge-induced colloid-colloid interactions onto effective hard-sphere–like interactions, the effect of the non-adsorbing polymer chains on the colloidal dispersion can be treated within the framework of the free-volume theory.

3 Generalised free-volume theory

3.1 Semi–grand-canonical potential

To compute the equilibrium phase diagram of mixtures of charged colloids and polymers, we need expressions for the free energy of the colloidal fluid and solid phases. Due to the fact that we have already mapped the screened electrostatic Coulomb interactions onto hard-sphere ones, we can apply a simple approach that successfully describes the stability of polymer-colloid mixtures [55,11]. Here, the colloid-polymer mixture is described in the semi–grand-canonical ensemble, where N_c colloidal particles (c) and N_p polymer chains are enclosed in the system with volume V at temperature T. The system is attached to a reservoir (r) of polymer chains (p), which is in osmotic equilibrium with the polymer solution in the system. Thus, the system is described by the $(N_\mathrm{c}, V, T, \mu_\mathrm{p}^\mathrm{r})$ ensemble, where $\mu_\mathrm{p}^\mathrm{r}$ is the chemical potential of the polymer chains in the reservoir. This $\mu_\mathrm{p}^\mathrm{r}$ determines the polymer number density $\rho_\mathrm{r} = N_\mathrm{p}/V$ in the system. The semi–grand-canonical potential is given by

$$\Omega(N_\mathrm{c}, V, T, \mu_\mathrm{p}^\mathrm{r}) = F(N_\mathrm{c}, V, T) - \int_{-\infty}^{\mu_\mathrm{p}^\mathrm{r}} \langle N_\mathrm{p}(\tilde{\mu}_\mathrm{p}^\mathrm{r})\rangle\, \mathrm{d}\tilde{\mu}_\mathrm{p}^\mathrm{r}\,. \quad (5)$$

The (canonical) free energy of the charged colloid dispersion in the absence of polymers is described by $F(N_\mathrm{c}, V, T)$; *i.e.*, $\Omega(N_\mathrm{c}, V, T, \mu_\mathrm{p}^\mathrm{r} \to -\infty) = F(N_\mathrm{c}, V, T)$. The brackets, $\langle\cdot\rangle$, beside the integral denote the semi–grand-canonical ensemble average, and the tilde indicates the integration variable.

We define the free-volume fraction as $\alpha(\rho_\mathrm{c}, \mu_\mathrm{p}^\mathrm{r}) = \langle V_\mathrm{free}\rangle/V = \rho_\mathrm{p}/\rho_\mathrm{p}^\mathrm{r}$, where V_free is the free volume in the system not occupied by the colloids and their depletion zones and $\rho_\mathrm{p}^\mathrm{r}$ is the reservoir polymer number density. Using the Gibbs-Duhem relation, $\rho_\mathrm{p}^\mathrm{r}\mathrm{d}\mu_\mathrm{p}^\mathrm{r} = \mathrm{d}\Pi_\mathrm{p}^\mathrm{r} = (\partial\Pi_\mathrm{p}^\mathrm{r}/\partial\rho_\mathrm{p}^\mathrm{r})\mathrm{d}\rho_\mathrm{p}^\mathrm{r}$, where $\Pi_\mathrm{p}^\mathrm{r}$ is the reservoir polymer osmotic pressure, we obtain

$$\omega(\eta_\mathrm{c}, y) = f(\eta_\mathrm{c}) - \int_0^y \alpha(\eta_\mathrm{c}, \mu_\mathrm{p}^\mathrm{r}(\tilde{y}))\frac{\partial\hat{\Pi}_\mathrm{p}^\mathrm{r}(\eta_\mathrm{c}, \mu_\mathrm{p}^\mathrm{r}(\tilde{y}))}{\partial\tilde{y}}\mathrm{d}\tilde{y}. \quad (6)$$

Here, we introduced the reduced semi–grand-canonical free-energy density $\omega = \beta\Omega v_0/V$ and the reduced canonical free-energy density $f = \beta F v_0/V$, where $1/\beta = k_\mathrm{B}T$ is the thermal energy and $v_0 = 4\pi a^3/3$ is the colloid volume. The relative reservoir polymer concentration is given by $y = \rho_\mathrm{p}^\mathrm{r}(4/3)\pi R_\mathrm{g}^3$, where R_g is the radius of gyration of a polymer coil. We also use the normalised osmotic pressure defined as $\hat{\Pi}_\mathrm{p}^\mathrm{r} = \beta\,\Pi_\mathrm{p}^\mathrm{r}(\eta_\mathrm{c}, \mu_\mathrm{p}(y))\,v_0$.

So far no approximation has been made. The contribution of the polymers to the free energy in the second term is now described by the (reservoir) polymer osmotic pressure, $\hat{\Pi}_\mathrm{p}^\mathrm{r}(\eta_\mathrm{c}, y)$, and the free-volume fraction, $\alpha(\eta_\mathrm{c}, y)$, accessible to the polymer chains.

We approximate $\alpha(\eta_\mathrm{c}, y)$ by an expression previously derived by Fortini *et al.* [50]

$$\alpha(\eta_\mathrm{c}, y) = (1-\eta_\mathrm{c})\exp(-b_1\gamma - b_2\gamma^2 - b_3\zeta - 3b_3\zeta^2 - 3b_3\zeta^3), \qquad (7)$$

where $\gamma = \eta_\mathrm{c}/(1-\eta_\mathrm{c})$, $\zeta = \eta_\mathrm{c}'/(1-\eta_\mathrm{c}')$, $b_1 = 3q_\mathrm{s} + 3q_\mathrm{s}^2$, $b_2 = 9q_\mathrm{s}^2/2$, and $b_3 = q_\mathrm{s}^3$. The size ratio $q_\mathrm{s} = \delta/a$ is the ratio of the depletion thickness δ around a spherical particle over a (see Fig. 1). For uncharged colloids, or infinite screening ($m \to 1$), the free-volume factor reduces to the hard-sphere one known from SPT [12,13]. A geometric interpretation of these factors in terms of fundamental measure theory has been given by Oversteegen and Roth [56]. The relative polymer concentration within the system, η_p, is given by $\eta_\mathrm{p} = \alpha(\eta_\mathrm{c}, y)\,y$.

We note that SPT is approximate, but surprisingly, the free-volume fraction from SPT appears to be rather accurate [20]. Brader *et al.* [57] have discussed possible ways to derive systematic expressions for the free-volume

fraction by first calculating the equilibrium properties of the effective one-component system where the polymer degrees of freedom have been integrated out. This could be done either theoretically or by using Monte Carlo computer simulations results. The polymer concentration and, thus, the free-volume fraction $\alpha(\eta_c, y)$ could then be obtained exactly using pair and higher-order distribution functions. An effective pair potential for mixtures of interacting (excluded-volume) polymer chains and colloids has been derived from computer simulations by Louis *et al.* [58], which might be used in such an approach. Thus, it is possible to test the extensively used SPT against exact computer simulations. There is a need for work in this direction to reveal how accurate SPT is for more complicated systems. The physical properties of the polymer solution will be discussed separately for ideal and interacting polymer in Sections 3.2, 3.3 and 3.4.

The canonical free energy of the effective hard-sphere system consists in the fluid phase of the ideal gas term

$$m\, f^{\mathrm{id}}(\eta_c) = \eta_c' \left[\ln(\eta_c' \Lambda_c^3/v_0) - 1\right], \tag{8}$$

where $\Lambda_c = h/\sqrt{2\pi m_c k_B T}$ is the thermal wavelength, with the colloid mass m_c, Planck's constant h, and the hard-sphere interaction term, which we describe by the Carnahan-Starling equation of state [59]

$$m f^{\mathrm{CS}}(\eta_c) = \frac{4{\eta_c'}^2 - 3{\eta_c'}^3}{(1-\eta_c')^2}. \tag{9}$$

Here the factor m appears because we have normalised the free energy by the bare colloid volume v_0 (see above).

The solid phase is assumed to have a face-centred-cubic (fcc) lattice structure. We use Wood's equation of state [60] to describe the free energy of the effective hard-sphere system [50]

$$m f^{\mathrm{Wood}}(\eta_c) = 2.1306\,\eta_c' + 3\,\eta_c' \ln\left(\frac{\eta_c'}{1-\eta_c'/\eta_c^{\mathrm{cp}}}\right) + \eta_c' \ln\left(\frac{\Lambda_c^3}{v_0}\right). \tag{10}$$

where $\eta_c^{\mathrm{cp}} = \pi\sqrt{2}/6$ is the fcc volume fraction for close packing. The integration constant (inside the first term on the right-hand side) is obtained from the absolute free energy of a hard-sphere crystal calculated from Monte Carlo simulations at $\eta_c = 0.576$ [61].

When fluid and solid phase coexist, the two phases are in thermal, mechanical, and chemical equilibrium. Thus, for a given polymer reservoir concentration, y, thermodynamic equilibrium is reached when the osmotic pressures

$$\hat{\Pi}_f(\eta_{c,f}, y) = \hat{\Pi}_s(\eta_{c,s}, y) \tag{11}$$

and the chemical potentials

$$\mu_f(\eta_{c,f}, y) = \mu_s(\eta_{c,s}, y) \tag{12}$$

of the fluid (f) and solid (s) phases are equal at the two different volume fractions, $\eta_{c,f}$ and $\eta_{c,s}$, respectively, where

$$\hat{\Pi}(\eta_c, y) = \eta_c^2 \frac{\partial(\omega(\eta_c, y)/\eta_c)}{\partial \eta_c} \tag{13}$$

and

$$\beta\mu(\eta_c, y) = \frac{\partial \omega(\eta_c, y)}{\partial \eta_c}. \tag{14}$$

A gas-like phase at low colloidal density coexists with a liquid-like phase at high colloidal density for equal osmotic pressures

$$\hat{\Pi}_g(\eta_{c,g}, y) = \hat{\Pi}_l(\eta_{c,l}, y), \tag{15}$$

and chemical potentials

$$\mu_g(\eta_{c,g}, y) = \mu_l(\eta_{c,l}, y). \tag{16}$$

The spinodal curve is found where the thermodynamic compressibility diverges at infinite wavelengths, *i.e.*, where

$$\frac{\partial^2 \omega(\eta_c, y)}{\partial \eta_c^2} = 0. \tag{17}$$

The binodal and spinodal terminate and merge at the critical point, where

$$\frac{\partial^2 \omega(\eta_c, y)}{\partial^2 \eta_c} = 0 \qquad \text{and} \qquad \frac{\partial^3 \omega(\eta_c, y)}{\partial^3 \eta_c} = 0. \tag{18}$$

The critical end-point marks the lowest polymer-to-colloid size ratio where a colloidal liquid is stable, and is found where the gas-liquid critical point coexists with the solid phase [62].

3.2 Dilute and semi-dilute polymer solutions

So far undetermined are the osmotic pressure, $\hat{\Pi}_p^r$, of the polymers in equation (6), and the depletion thickness δ, which enters the free-volume fraction $\alpha(\eta_c, y)$, equation (7), through the size ratio $q_s = \delta/a$. For small polymer-to-colloid size ratios, $q \lesssim 0.4$, the relevant part of the phase diagram lies below the polymer overlap concentration ($y < 1$). Then interactions between the polymers are not essential to properly describe the phase diagram and it is still sufficient to approximate the polymer-induced osmotic pressure by the ideal-gas law as assumed in the seminal work by Lekkerkerker *et al.* [11]. Furthermore, the depletion thickness takes a value close to R_g in dilute polymer solutions. In dilute polymer solutions, the depletion thickness near a flat plate, δ_0, is given by [63,45]

$$\delta_0 = pR_g, \quad \text{with} \quad p = \begin{cases} 2/\sqrt{\pi} & \text{in a } \theta\text{-solvent,} \\ 2x/\sqrt{\pi} & \text{in a good solvent,} \end{cases} \tag{19}$$

where $x = 3/4 + 3\ln(2)/8 + \pi/8 - \pi/\sqrt{48} = 0.9492$. When the polymers have a similar or larger size with respect to the colloidal particles, $q \gtrsim 1$, the polymer concentrations where phase transitions occur, are of the order of and above the polymer overlap concentration (compare, *e.g.* Fig. 4b and c in [43]). Thus, for $q \gtrsim 0.4$ interactions between the polymer segments should be accounted for. In the semi-dilute concentration regime, the depletion thickness becomes the concentration-dependent correlation length $\xi \sim y^{-\tau}$, with $\tau = 1$ for θ-solvents

and $\tau = 0.77$ for good solvents [64]. To incorporate the crossover from dilute to the semi-dilute polymer concentrations, Fleer *et al.* [52] have derived phenomenological expressions for the polymer concentration-dependent depletion thickness and the polymer-induced osmotic pressure by interpolating between the exactly known dilute limit and scaling relations valid for semi-dilute polymer concentrations using combination rules.

For the osmotic pressure they found [52]

$$\hat{\Pi}_{\rm p}^{\rm r}(q,y) = q^{-3}\left(y + A\,y^{3\tau}\right). \qquad (20)$$

The de Gennes scaling exponent τ and the parameter A depend on the solvent quality and will be specified in Sections 3.3 and 3.4. In the dilute limit, $y \ll 1$, equation (20) reduces to the osmotic pressure of an ideal polymer solution, $\hat{\Pi}_{\rm p}^{\rm r} = q^{-3}y$, and in the semi-dilute regime it recovers the scaling relation $\hat{\Pi}_{\rm p}^{\rm r} \sim \xi^{-3} \sim q^{-3}y^{3\tau}$ [64].

The depletion thickness for dilute and semi-dilute polymer solutions next to a flat plate, $\delta_{\rm p}$, was obtained previously [51,52,65]

$$\delta_{\rm p}/\delta_0 = \left(1 + B y^{2\tau}\right)^{-1/2}, \qquad (21)$$

where B is a parameter which again depends on the solvent quality. In the dilute limit ($y \to 0$), $\delta_{\rm p}$ reduces to δ_0, and in the semi-dilute limit it recovers the scaling relation $\delta_{\rm p} \sim y^{-\gamma}$ [64].

We also have to account for curvature effects to find an accurate description for the depletion thickness, δ, around the spherical colloidal particles. For ideal polymer chains, Louis *et al.* [66] and Aarts *et al.* [43] derived the relation between δ as a function of the depletion thickness at a flat plate in *dilute* polymer solutions, δ_0, using the density profile around a sphere [44,67]

$$q_{\rm s}^{\rm (mf)}(q_0) = \left(1 + 3\,q_0 + \frac{3\pi}{4}\,q_0^2\right)^{1/3} - 1\,, \qquad (22)$$

where $q_0 = \delta_0/a$ and $q_{\rm s} = \delta/a$. This result is valid for dilute polymers in a θ-solvent. Hanke *et al.* [45] have derived an equivalent relation for polymer chains in the excluded-volume limit (*i.e.*, for polymer chains with excluded-volume monomer-monomer interactions (ev)),

$$q_{\rm s}^{\rm (ev)}(q_0) = \left(1 + 3q_0 + 3c_2q_0^2 - 3c_3q_0^3 + \ldots\right)^{1/3} - 1\,, \quad (23)$$

where $c_2 = \pi(1 - 5\pi/8 + 17/36 + \pi\sqrt{3}/4)/(4\,x^2) = 0.7576$ and $c_3 = \pi(1673\pi/48 - 551/15 - 40\sqrt{3}/\pi)/(24x^3) = 0.0325$. In Figure 2, we plot $q_{\rm s}$ as a function of q, where $q = q_0/p$ according to equation (19). The lower curve corresponds to polymers in a good solvent (Eq. (23)) and the upper curve is the result for a θ-solvent (Eq. (22)). As proposed by Fleer and Tuinier [51,68], $q_{\rm s}$ can be approximated by simpler power laws

$$q_{\rm s}^{\rm (mf)}(q_0) = 0.842\,q_0^{0.9}, \qquad (24)$$

and

$$q_{\rm s}^{\rm (ev)}(q_0) = 0.814\,q_0^{0.88}. \qquad (25)$$

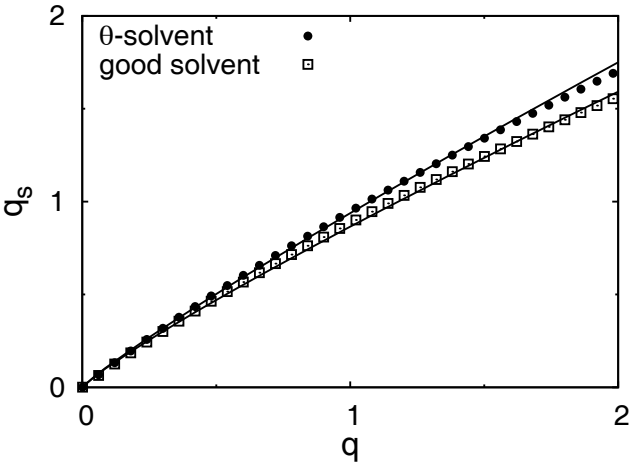

Fig. 2. Normalised depletion thickness around a sphere, $q_{\rm s} = \delta/a$, as a function of the reduced radius of gyration, $q = R_{\rm g}/a$. The dots correspond to polymer chains in a θ-solvent (Eq. (22)) and the squares describe interacting polymer chains in good solvent (Eq. (23)). The solid curves indicate the power law fits (Eqs. (24) and (25), respectively) to the analytical expressions for polymer chains in a θ-solvent (Eq. (22)) and in a good solvent (Eq. (23)), respectively.

These are indicated in Figure 2 by dots (mean-field chains) and squares (excluded-volume chains). As expected, the depletion thickness around a sphere is smaller compared to the depletion thickness close to a flat plate. Furthermore, the depletion thickness due to polymer chains in a good solvent (excluded-volume chains) is smaller as compared to polymers in a θ-solvent. The deviations become more pronounced with increasing q. The $q > 2$ regime is, however, less relevant as we shall see. In addition, we show the influence of q on the depletion thickness around a sphere, δ, relative to the radius of gyration $R_{\rm g}$ for good and θ-solvent conditions in Figure 3. As can be seen clearly, $\delta/R_{\rm g}$ decreases with increasing q and is well below unity if q exceeds unity.

3.3 Polymer solutions in a θ-solvent (mean-field approximation)

For polymer chains in a θ-solvent the scaling exponent τ takes its mean-field value $\tau = 1$. The parameters that follow from the combination rules that link the semi-dilute regime of the osmotic pressure and the depletion thickness towards zero polymer volume fraction are $A = 4.1$ and $B = 5.94$ [52], respectively. The polymer concentration derivative of the reduced osmotic pressure is

$$\frac{\partial \hat{\Pi}_{\rm p}^{\rm r}(q,y)}{\partial y} = q^{-3}[1 + 12.3\,y^2], \qquad (26)$$

and the depletion thickness-to-colloid radius size ratio is

$$q_{\rm s}(q,y) = 0.938\,\left(q/\sqrt{1 + 5.94\,y^2}\right)^{0.9}. \qquad (27)$$

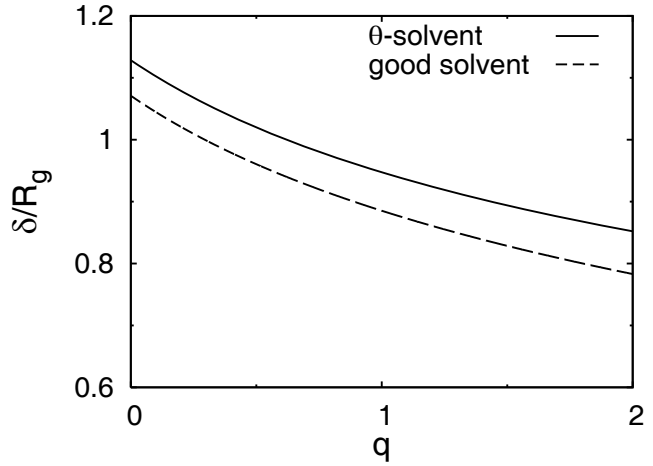

Fig. 3. Influence of the polymer-to-colloid size ratio $q = R_g/a$ on the depletion thickness around a sphere in units of the radius of gyration, δ/R_g. The solid curve describes the size ratio dependence of δ/R_g for polymer chains in a θ-solvent and the dashed one the influence of the curvature for good solvent conditions.

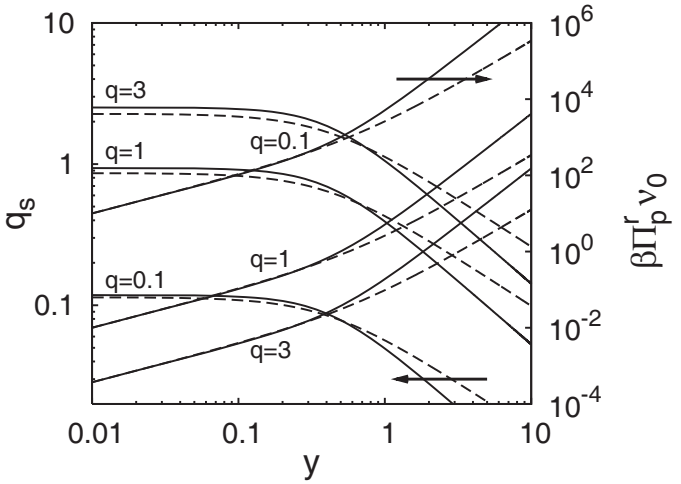

Fig. 4. Influence of the polymer concentration y on the relative depletion thickness around a sphere, $q_s = \delta/a$, and on the reduced polymer osmotic pressure $\hat{\Pi}_p = \beta\,\Pi_p^r\,\nu_0$. The solid curves describe the influence of y on q_s and $\hat{\Pi}_p$, respectively, for polymer chains in θ-solvent and the dashed curves for polymers in good solvent.

Equation (27) follows directly by replacing q_0 with the reduced depletion thickness for dilute *and* semi-dilute polymer solution, δ_p/a, introduced in equation (21), and using equation (19).

3.4 Interacting polymer solutions in good solvent

In a semi-dilute polymer solution, the de Gennes scaling exponent τ equals 0.77 under good solvent conditions. The parameters A and B now read $A = 1.615$ and $B = 3.95$ [52]. Therefore, we have

$$\frac{\partial \hat{\Pi}_p^r(q,y)}{\partial y} = q^{-3}[1 + 3.73\,y^{1.31}] \qquad (28)$$

and

$$q_s(q,y) = 0.865\,\left(q/\sqrt{1 + 3.95\,y^{1.54}}\right)^{0.88}. \qquad (29)$$

Note that in contrast to the classical FVT [11], $\partial\hat{\Pi}_p^r/\partial y$ and q_s in equations (26)–(29) now depend on the polymer concentration y.

In Figure 4, the effective size ratio q_s is given as a function of the polymer concentration y for $q = 0.1$, 1 and 3. The solid curves describe polymer chains in θ-solvent and the dashed curves polymers under good solvent conditions. The effective size ratio $q_s = \delta/a$ is nearly independent of y at small polymer concentrations ($y \lesssim 0.1$) and decreases rapidly with increasing y. It follows that the effective size ratio is smaller for polymer chains in a good solvent as compared to chains in a θ-solvent for low polymer concentrations, but decreases less rapidly with increasing y so that for high concentrations the effective size ratio in a good solvent is larger than q_s in a θ-solvent. Also shown in Figure 4 is the reduced polymer-induced osmotic pressure $\beta\Pi_p^r v_0$, which describes the osmotic work to insert a particle without depletion layer. As expected, the work required for inserting a colloidal particle increases with increasing polymer concentration. However, $\beta\Pi_p^r v_0$ increases more rapidly for polymer chains in a θ-solvent as for chains in good solvent. We note that the polymer concentration is normalised with the overlap concentration. The overlap concentration for polymer chains in a good solvent is significantly smaller as for θ chains due to chain swelling.

4 Results and discussion

4.1 Phase behaviour of uncharged colloid-polymer mixtures: Comparison with computer simulation results

We first compare the generalised free-volume theory with computer simulation data by Bolhuis *et al.* [41,69] on (uncharged) colloid-polymer mixtures. In [41] they computed the gas-liquid phase coexistence curves for mixtures of hard spheres plus a polymer solution with interacting chains modelled as Gaussian cores ($q = 0.34$, 0.67 and 1.05) investigating the colloid limit ($q < 1$) and a colloid-polymer mixture with equal size. Gas-liquid binodals in the protein limit ($q > 1$) were computed for hard spheres plus excluded-volume chains on a discrete lattice using Monte Carlo (MC) techniques for $q = 3.86$, 5.58 and 7.78. In Figure 5 the simulation data with size ratios $q = 0.34$, $q = 0.67$ and $q = 1.05$ are compared with the predicted gas-liquid coexistence curves from generalised free-volume theory (GFVT). The theoretically predicted gas-liquid coexistence curve agrees well for $q = 0.34$ with the computer simulation data. With increasing size ratios (*i.e.*, at $q = 0.67$ and $q = 1.05$) the binodals predicted from GFVT start to deviate slightly from the simulation data. In fact, the polymer concentration at which phase separation first occurs is slightly overestimated by GFVT.

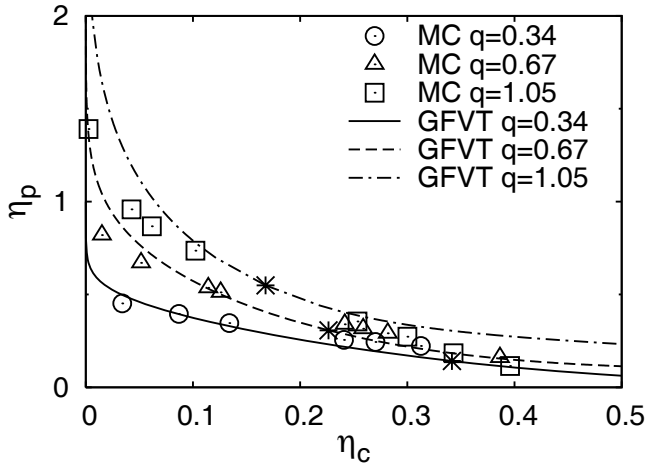

Fig. 5. Gas-liquid coexistence curves for size ratios q as indicated in the colloid limit ($q \lesssim 1$) and for equal size for mixtures of interacting polymer in a good solvent plus hard-sphere colloids. The open symbols are results from computer simulations by Bolhuis *et al.* [69] using a Gaussian core model for the polymer chains. The curves are calculated gas-liquid binodals using generalised free-volume theory. The asterisks indicate the theoretical critical point.

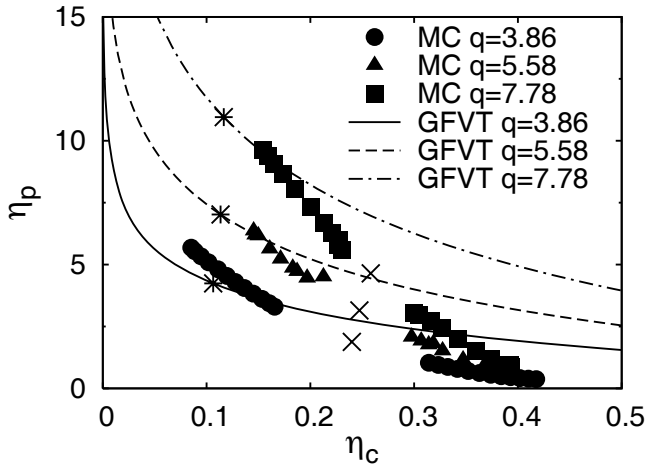

Fig. 6. Gas-liquid coexistence curves at different size ratios q in the protein limit ($q > 1$) for hard spheres and interacting polymer chains in a good solvent. The coexistence curves are calculated from generalised free-volume theory. The asterisks are the critical points calculated from theory. The solid binodal data points are taken from Bolhuis *et al.* [69], and the crosses indicate critical points extracted from these computer simulation data.

This deviation increases with increasing colloid volume fraction. In Figure 6 the calculated gas-liquid phase coexistence curves from GFVT are plotted together with MC data in the protein limit ($q = 3.86$, $q = 5.58$ and $q = 7.78$), and larger deviations are found. At low η_c the binodals are underestimated by GFVT (*i.e.*, phase separation is predicted at too low polymer volume fractions), whereas the stability region of the homogeneous colloid-polymer mixture is significantly overestimated at high η_c. The colloidal volume fraction at the critical point is underestimated and the critical polymer volume fraction is overestimated by GFVT by a factor of two. Thus, we conclude that GFVT describes colloid-polymer mixtures in the colloid limit reasonably well, but is less adequate to quantitatively predict the MC simulation results of the phase coexistence curves in the protein limit. This limitation of GFVT for size ratios of $q \geq 1$ could be due to the fact that the polymers are treated within SPT as a small perturbation to the hard-sphere colloidal reference system. In fact, one assumes that the configurations of the colloids do not change if a small polymer chain is inserted. Obviously, this assumption holds only if the polymer coil is small compared to the colloid size. We note that computer simulations are of course not exact but also approximate real systems. PRISM predicts critical colloid volume fractions in the protein limit that are quite close to GFVT predictions [68]. Besides some quantitative mismatch, it has been shown by Fleer and Tuinier [51] that GFVT predicts the q-scaling behaviour correctly [69]. In addition, the critical colloid volume fraction observed within GFVT is nearly constant as found in MC simulation and PRISM. The theory and computer simulations show that the critical polymer concentration increases with increasing q.

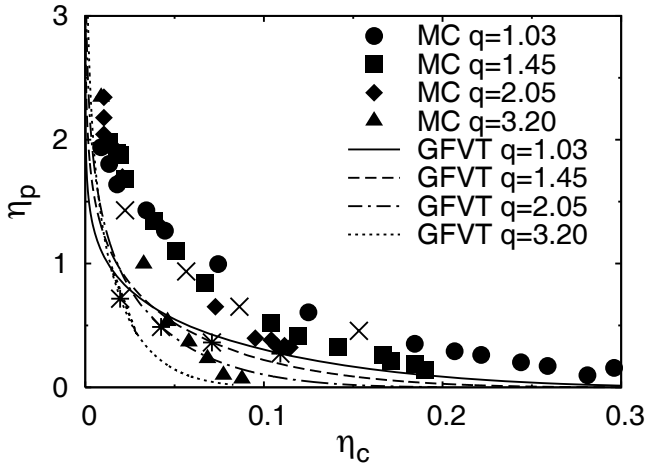

Fig. 7. Gas-liquid coexistence curves at different size ratios q for ideal, non-interacting polymer chains. The coexistence curves are calculated from generalised free-volume theory. The asterisks mark the GFVT critical points. The solid data binodal points are taken from Bolhuis *et al.* [69], with the crosses indicating the extracted critical points from these MC computer simulation data.

In Figure 7 we compare binodals for mixtures of ideal (non-interacting) polymers and colloids from MC [69] and GFVT. The expressions for ideal polymers are obtained from equation (26) and equation (27) for $y \to 0$. In contrast to interacting polymer chains, the critical volume fraction shifts to smaller values with increasing q, while the critical polymer volume fraction increases at the same time as observed in interacting polymers solutions. But whereas the region where a stable homogeneous colloid-polymer mixture is increasing in interacting polymer solutions, the area underneath the binodal shrinks with increasing q in an ideal polymer solution. In summary, we

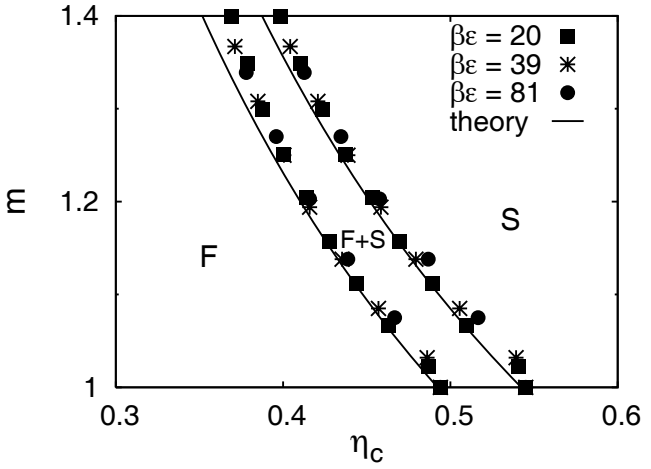

Fig. 8. Fluid-solid coexistences for various values of the effective volume fraction factor m on the fluid-solid coexistence regime. The capital letters indicate the phase region where a stable fluid (F) or a stable solid phase (S) is observed. A fluid phase coexists with a fcc solid phase in the gap between the two curves (F + S). The solid curves are calculated from our free-energy expressions for the weakly charged spheres (Eqs. (8–10)). The symbols correspond to Monte Carlo simulation data of Hynninen and Dijkstra [71] for three different contact values, $\beta\epsilon$, of the repulsive pair interaction potential (Eq. (1)); see legend. The curves represent the binodal curves calculated using the free-energy expressions of equations (9) and (10) for the fluid and fcc solid, respectively.

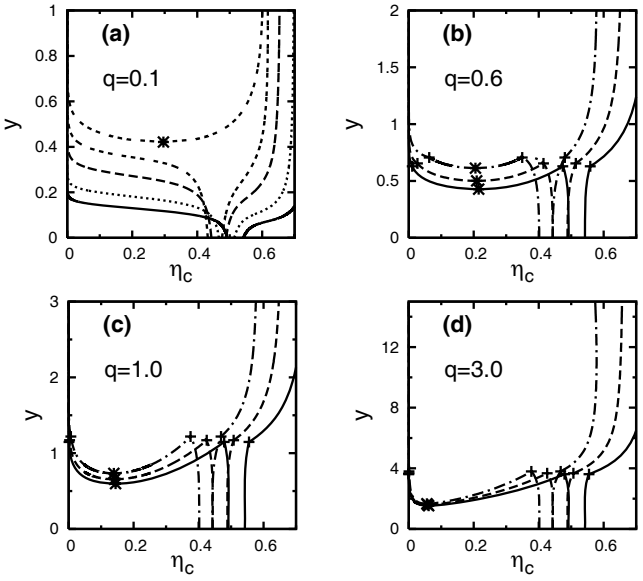

Fig. 9. Phase diagram for mixtures of colloids carrying screened electrostatic charges and polymers at the θ condition. The solid curves describe uncharged (infinite screening) colloidal dispersions ($m = 1.0$, or $\kappa a \to \infty$, respectively). The dotted curve is obtained for $m = 1.054$ (or, $\kappa a = 100$ for $\beta\epsilon = 20$) and the dashed curves for $m = 1.110$ (or, $\kappa a = 50$ for $\beta\epsilon = 20$). The short-dashed curve describes the phase coexistence obtained for $m = 1.138$ (or, $\kappa a = 40$ for $\beta\epsilon = 20$) and the dashed-dotted curves represent the phase coexistence curves for $m = 1.225$ (or, $\kappa a = 25$ for $\beta\epsilon = 20$). The plusses indicate the triple points and the asterisks mark the critical points of the gas-liquid phase transition. Note that the reservoir polymer concentration is plotted as ordinate. Thus, the tie-lines are parallel to the abscissa.

note that the general trends of the phase behaviour are rendered by GFVT even in the protein limit. Thus, we conclude that GFVT gives quantitative predictions for $q \lesssim 1$ (colloid limit) and describes polymer-colloid mixtures qualitatively for $q > 1$ (protein limit), capturing the general trends correctly.

Finally, we note that there is an urgent need for simulations of the fluid-solid and gas-liquid-solid phase behaviour to compare with our analytical theory.

4.2 Phase behaviour of charged colloid-polymer mixtures

We now turn to the main item of this paper: the phase behaviour of charged colloidal particles and polymers in either a good or a θ-solvent.

First, we focus on a pure hard-sphere dispersion without charges ($1/\kappa = 0$, or, correspondingly, $m = 1.0$) and without any added polymers ($y = 0$). In that case we recover the hard-sphere fluid-solid phase coexistence at $\eta_c = 0.492$ (fluid) and $\eta_c = 0.542$. These values agree well with the freezing and melting volume fractions of 0.494 and 0.545, respectively, observed in computer simulations [70]. If the colloidal particles are charged ($m > 1$), the effective volume increases (see Eq. (4)), and thus, the freezing and melting volume fractions shift to lower values as shown in Figure 8. Here, the data points are the fluid-solid coexistence data from Hynninen and Dijkstra [71] obtained from Monte Carlo simulations for repulsive contact potentials of $\beta\epsilon = 20$, 39 and 81. As can be seen in Figure 8 the data collapse for different $\beta\epsilon$-values when m is plotted on the ordinate as expected.

We now want to elucidate the influence of the solvent quality on the (global) phase behaviour and, secondly, the interplay between charge-induced repulsions *versus* polymer-induced attractions. Figures 9 and 10 show the phase behaviour for four different size ratios ($q = 0.1$, $q = 0.6$, $q = 1.0$ and $q = 3.0$) for polymers in a θ-solvent (Fig. 9) and under good solvent conditions (Fig. 10), respectively. Note that we plot the phase diagrams in the η_c-y plane with y the normalised reservoir polymer concentration. Thus, the tie-lines (not shown) are horizontal.

Adding non-adsorbing polymers induces an attractive interaction and for small q the fluid-solid coexistence region widens upon increasing the polymer concentration (see, *e.g.*, Fig. 9(a) and Fig. 10(a)). For $q = 0.1$, the depletion-induced attractive interactions are too short ranged to induce a stable gas-liquid phase separation and only a stable (or equilibrium) fluid-solid phase separation is observed. The metastable gas-liquid coexistence curve lies within the fluid-solid coexistence region as shown for $m = 1.138$ in Figure 9(a). As shown in Figure 9(a) and Figure 10(a), the fluid-solid coexistence curves shift to higher reservoir polymer concentration y with increasing

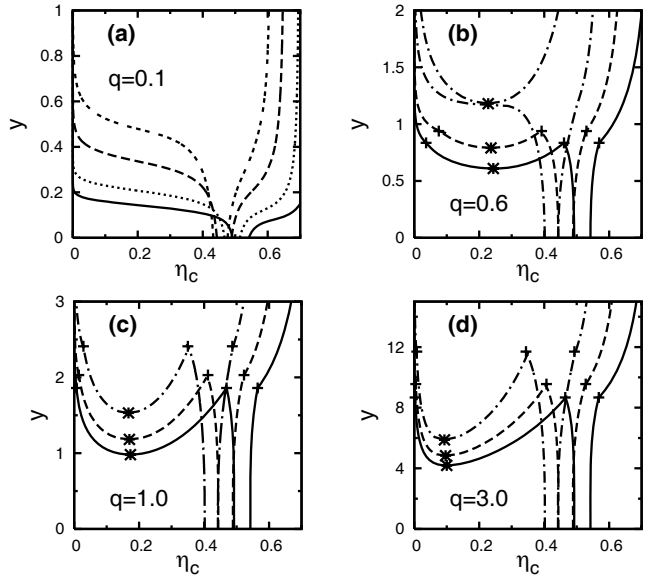

Fig. 10. Phase diagram for mixtures of colloids carrying screened electrostatic charges and polymers at good solvent conditions. The solid curves describe uncharged (infinite screening) colloidal dispersions ($m = 1.0$, or $\kappa a \to \infty$, respectively). The dotted curve is obtained for $m = 1.054$ (or, $\kappa a = 100$ for $\beta\epsilon = 20$) and the dashed curves for $m = 1.110$ (or, $\kappa a = 50$ for $\beta\epsilon = 20$). The short-dashed curve describes the phase coexistence obtained for $m = 1.138$ (or, $\kappa a = 40$ for $\beta\epsilon = 20$) and the dashed-dotted curves represent the phase coexistence curves for $m = 1.225$ (or, $\kappa a = 25$ for $\beta\epsilon = 20$). The plusses indicate the triple points and the asterisks mark the critical points of the gas-liquid phase transition. Note that the reservoir polymer concentration is plotted as ordinate. Thus, the tie-lines are parallel to the abscissa.

Debye screening length κ^{-1}, or, correspondingly, with increasing m. Hence, the one-phase region underneath the fluid-solid coexistence curves, where a stable mixture at low polymer and colloid concentrations exists, increases with increasing m. This behaviour is expected since the short-ranged depletion-induced interactions are being more and more compensated by the increasing electrostatic repulsions with decreasing κ.

For larger q the depletion-induced attraction becomes longer ranged and a stable gas-liquid phase coexistence is manifested. The polymer-to-colloid size ratio at which this transition from a metastable to a stable phase coexistence between two fluids with low and high colloidal density takes place is described by the critical end-point [62]. This quantity marks the boundary condition for a colloidal liquid. The values that characterise the critical end-point obtained from GFVT are summarised in Table 1 for colloids mixed with polymer in a θ-solvent and in a good solvent. Here, $m = 1$ corresponds to the hard-sphere case, $\kappa \to \infty$, and $m = 1.110$ corresponds to a inverse screening length of $\kappa a = 50$, and $m = 1.225$ to $\kappa a = 25$, with $\beta\epsilon = 20$ throughout.

As shown in Figures 9(b,c,d) and Figures 10(b,c,d), in the hard-sphere case of infinite screening, ($m = 1$) and for $m = 1.110$, a gas-liquid coexistence curve manifests itself

Table 1. Values obtained from the generalised free-volume theory that characterise the critical end-point for colloids mixed with polymers in a θ-solvent (upper part) and in a good solvent (lower part). The effect of charges is convoluted in the parameter m (see text). For $m > 1$ the colloids are charged.

	m	$q^{\rm cep}$	$q_{\rm s}^{\rm cep}$	$y^{\rm cep}$	$\alpha^{\rm cep}$	$\eta_{\rm c}^{\rm cep}$
θ-solvent	1.0	0.34	0.29	0.31	0.36	0.32
	1.11	0.40	0.30	0.43	0.43	0.27
	1.225	0.49	0.30	0.59	0.51	0.23
Good solvent	1.0	0.39	0.27	0.43	0.38	0.32
	1.11	0.47	0.27	0.68	0.46	0.27
	1.225	0.61	0.25	1.21	0.57	0.22

at low reservoir polymer concentrations with respect to the fluid-solid phase coexistence curve for $q = 0.6$, 1.0, and 3.0. In contrast, Figure 10(b) ($q = 0.6$, $m = 1.225$) shows a metastable gas-liquid coexistence curve (dashed-dotted curve), which nearly touches the fluid-solid coexistence curve. For $q = 1.0$ and $q = 3.0$ the fluid-solid curves are stable for $m = 1.225$.

In the hard-sphere limit (solid curves) and for small q (*i.e.*, $q = 0.1$), there is nearly no difference between the fluid-solid phase coexistence curves for polymers in a θ-solvent and for polymers in a good solvent (compare Fig. 9(a) with Fig. 10(a)). The critical colloid volume fraction is also similar for both solvency conditions (see Figs. 13 and 14, and the discussion on this later on). With increasing q the stability of the mixed phase increases. Furthermore, the binodals are shifted to higher reservoir polymer concentrations for polymers in good solvent conditions as compared to chains in a θ-solvent at larger size ratios. To induce a gas-liquid phase transition at good solvent conditions, y is about a factor of two higher than in case of polymers in a θ-solvent. Similar trends have been observed by Schmidt and Fuchs [42].

As stated before, electrostatic repulsions between the colloids in general stabilise the homogeneous phase. Hence, more polymers have to be added to induce sufficient attraction, and hence, the phase separation curves shift to higher y-values as observed in all phase diagrams. Interestingly, the influence of electrostatic repulsions on the location of the phase boundaries is much more pronounced in case of good solvent conditions compared to θ-solvent conditions. The effect of the solvent quality on the phase behaviour becomes especially apparent in the protein limit (*i.e.*, $q = 3.0$), see Figure 9(d) and Figure 10(d). In case of a θ-solvent, the binodal at low colloid volume fraction is almost unaffected by the electrostatic repulsion (Fig. 9(d)), whereas in a good solvent the homogeneous fluid phase becomes considerably stabilised with increasing m (Fig. 10(d)). This is due to the fact that $q_{\rm s}$ is much smaller than q at the binodal for $q = 3.0$ especially under good solvent conditions. To make this explicit, we give some values at the gas-liquid critical point where $q_{\rm s} = 0.5$ at $m = 1.0$ and $q_{\rm s} = 0.4$ at $m = 1.225$ for colloidal spheres plus polymer chains in a good solvent, while in a θ-solvent, $q_{\rm s} = 0.7$ at $m = 1.0$ and $q_{\rm s} = 0.7$ at $m = 1.225$.

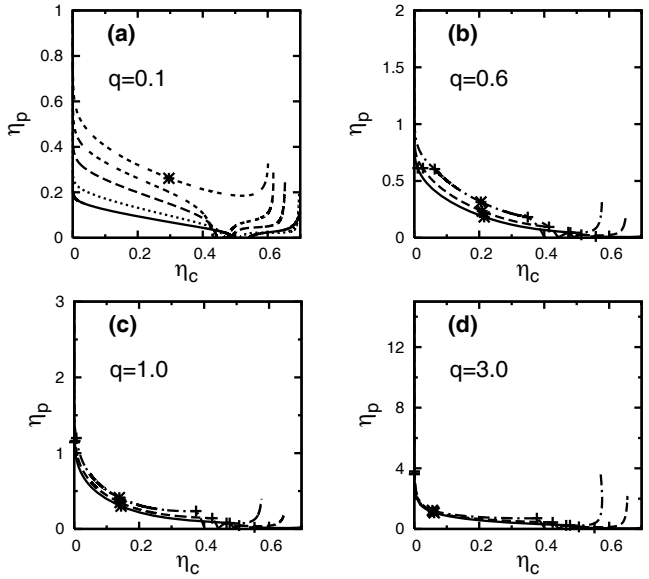

Fig. 11. Phase diagram for mixtures of colloids carrying screened electrostatic charges and polymers at the θ condition. In contrast to Figure 9, the coexistence curves are plotted here in the $\eta_{\rm P}$-$\eta_{\rm c}$ plane with the system polymer concentration. The solid curves describe uncharged (infinite screening) colloidal dispersions ($m = 1.0$, or $\kappa a \to \infty$, respectively). The dotted curve is obtained for $m = 1.054$ (or, $\kappa a = 100$ for $\beta\epsilon = 20$) and the dashed curves for $m = 1.110$ (or, $\kappa a = 50$ for $\beta\epsilon = 20$). The short-dashed curve describes the phase coexistence obtained for $m = 1.138$ (or, $\kappa a = 40$ for $\beta\epsilon = 20$) and the dashed-dotted curves represent the phase coexistence curves for $m = 1.225$ (or, $\kappa a = 25$ for $\beta\epsilon = 20$). The plusses indicate the triple points and the asterisks mark the critical points of the gas-liquid phase transition.

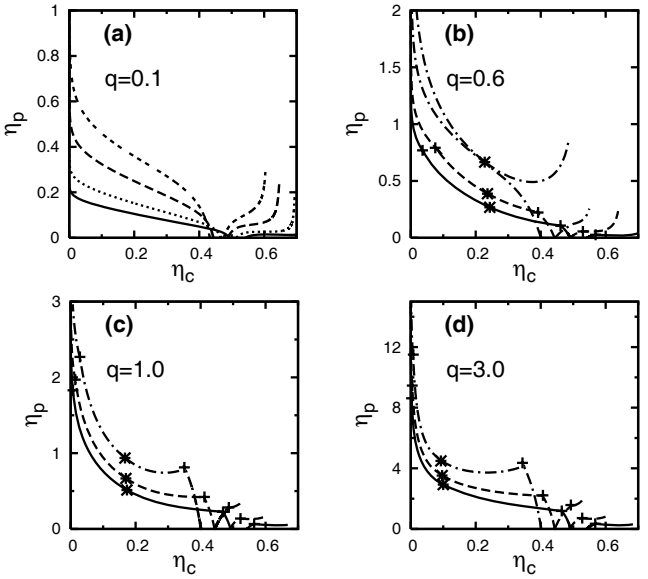

Fig. 12. Phase diagram for mixtures of colloids carrying screened electrostatic charges and polymers at good solvent conditions. In contrast to Figure 10, the coexistence curves are plotted here in the $\eta_{\rm P}$-$\eta_{\rm c}$ plane with the system polymer concentration. The solid curves describe uncharged (infinite screening) colloidal dispersions ($m = 1.0$, or $\kappa a \to \infty$, respectively). The dotted curve is obtained for $m = 1.054$ (or, $\kappa a = 100$ for $\beta\epsilon = 20$) and the dashed curves for $m = 1.110$ (or, $\kappa a = 50$ for $\beta\epsilon = 20$). The short-dashed curve describes the phase coexistence obtained for $m = 1.138$ (or, $\kappa a = 40$ for $\beta\epsilon = 20$) and the dashed-dotted curves represent the phase coexistence curves for $m = 1.225$ (or, $\kappa a = 25$ for $\beta\epsilon = 20$). The plusses indicate the triple points and the asterisks mark the critical points of the gas-liquid phase transition.

Actually, the depletion thickness becomes of the order of the correlation length ξ for $q > 1$ (protein limit) in semi-dilute polymer solutions and decreases with increasing y. Thus, even a short-ranged repulsion due to charges might be sufficient to compensate the depletion-induced attractions and, therefore, can have a large influence on the phase diagram.

As a practical illustration, we plot the phase diagrams in Figures 11 and 12 for $q = 0.1$, 0.6, 1 and 3 in the $\eta_{\rm P}$-$\eta_{\rm c}$ representation with the *system* polymer concentration. These can be compared with experimental data.

To discuss the influence of electrostatic repulsion and the effect of different solvent qualities on characteristic points that quantify the global phase behaviour, *i.e.* the critical point, the critical end-point, and the triple point, we turn to Figures 13 and 14. Here, these characteristic state points are plotted as a function of the colloid-to-polymer size ratio $1/q$. Pluses (+) indicate the triple points and open diamonds ($\diamond$) the critical points. The critical end-points are marked by an asterisk ($*$). The curves interconnect the volume fractions of the gaseous, liquids and solid phase coexisting at the triple point as a function of q. A curve connecting several critical points as a function of q is called a critical line. The full curve interconnects characteristic state points for $m = 1.0$, and the dotted and dashed curves link the triple and critical points for $m = 1.110$ and $m = 1.225$, respectively. The critical end-points shift to larger q-values with increasing electrostatic repulsions, which is at variance with Figures 9 and 10. In addition, the volume fractions at the triple point and the critical points reduce to lower values when increasing the electrostatic repulsions. Due to the fact that the depletion thickness reduces by increasing the solvent quality, gas-liquid phase separation sets in at larger q-values in case of interacting polymers in a good solvent. Adding electrostatic repulsions strongly reduces the liquid window, *i.e.*, the range of colloid concentrations and polymer-to-colloid size ratios where a colloidal liquid exists. When comparing this with mixtures of charged spheres with non-interacting polymers, one observes that the phase diagrams with interacting polymers are shifted to significantly higher polymer concentrations for $q > 0.5$ [50].

As can be seen in Figures 13 and 14, the critical colloid volume fraction, $\eta_{\rm c}^{\rm crit}$, converges towards a finite value in the protein limit (*i.e.*, for $q \to \infty$), as observed by Bolhuis *et al.* [41,69]. But whereas $\eta_{\rm c}^{\rm crit}$ approaches a constant value in case of a θ-solvent (Fig. 13), $\eta_{\rm c}^{\rm crit}$ has a minimum for $q = 3.0$ and then increases again slightly for $q \to \infty$ in case of a good solvent (Fig. 14). This observation can be

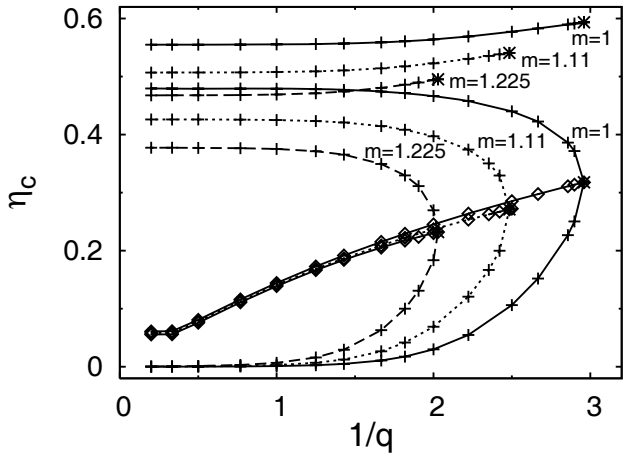

Fig. 13. Triple points (+), critical points (⋄) and critical endpoints (∗) as a function of the inverse of polymer-to-colloid size ratio, $1/q = a/R_g$, for mixtures of non-adsorbing polymers in a θ-solvent and uncharged colloids ($m = 1.0$, solid curve) and for colloids carrying screened electrostatic charges ($m = 1.110$, dotted curve and $m = 1.225$, dashed curve).

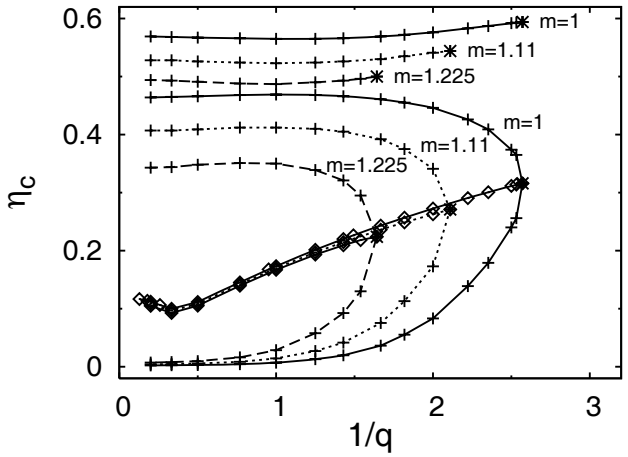

Fig. 14. As in Figure 13 but now for interacting polymers in a good solvent.

explained again by the fact that $\eta_c^{\rm crit}$ is determined by the range of attraction, *i.e.* by the effective polymer-to-colloid size ratio. In the semi-dilute limit the effect size δ becomes of the order of ξ ($\xi \ll R_{\rm g}$) and, thus, becomes independent of q. Therefore, $\eta_c^{\rm crit}$ approaches a constant for $q \to \infty$. In case of a θ-solvent, the depletion-induced range of attraction, δ, is, even for $q \to \infty$, larger than the range of repulsion caused by the hard-sphere plus Coulomb repulsion, and, hence $\eta_c^{\rm crit}$ continuously decreases for increasing q. In contrast, in case of a good solvent, δ is small to such a degree (compare Fig. 3) that it is overcompensated by the repulsive interactions so that $\eta_c^{\rm crit}$ goes through a minimum at $q \approx 3$ and then slightly increases for larger q-values (Fig. 14). We note, further, that the dominant contribution to the repulsive interactions is due to the hard-sphere contribution for all κ-values under investigation. Therefore, $\eta_c^{\rm crit}$ becomes independent of m for $q \to \infty$ in both cases.

As a critical remark, we note that conceptual difficulties arise by mapping the screened electrostatic Coulomb interactions onto hard-sphere ones. Hence, one has to be aware of the problems which might occur in conjunction with such a procedure as indicated in the following (see also [72] for a general discussion on effective pair interaction potentials). In general, as long the polymer chains do not carry charges (*i.e.*, as long as we do not consider polyelectrolytes as depletion agents) the polymer-induced depletion interactions are driven by geometrical, excluded-volume effects and are "entropy driven" [73]. On the other hand, the repulsive pair interactions of the charged colloids are transmitted by an electric field caused by surface and (micro-ionic) space charges. Thus, polymer-induced depletion effects and screened electrostatic interactions are of a different physical origin, and, hence, independent of each other. However, by mapping the screened electrostatic Coulomb interactions onto effective hard-sphere ones, the two physically independent interactions becomes geometrically related. In particular, it is unclear whether the depletion thickness must be added to the effective hard-sphere particle or to the bare one, or whether the polymer size has to be scaled so that the colloid-polymer mixtures remains additive as proposed by Denton and Schmidt [49]. Such a mapping obviously fails completely if the range of the repulsive screened Coulomb interactions exceeds the range of attraction induced by the polymer chains in solution. Thus, our model describes mixtures of charged colloids and polymers dispersed in an electrolyte solvent only in the limit of weakly charged or, respectively, highly screened colloidal particles. This procedure might lead to non-physical predictions when used *ad hoc* without precaution.

4.3 A mixture of globulin proteins and dextran in an aqueous salt solution

As a practical example, we now compare our theoretical results with the phase behaviour of globulin dispersions with added non-adsorbing dextran. Fortini *et al.* [50] have shown that mapping the screened electrostatic repulsive interactions onto effective hard-sphere ones is accurate for $m \lesssim 1.225$ (see [50], Fig. 2, p. 7789, and Fig. 8 in this work). Such high salt conditions are often encountered to screen the Coulomb interactions and, thus, to induce crystallisation. Hoskins *et al.* [74] have experimentally determined the phase behaviour of mixtures of globulin and dextran which falls into that regime. In particular, they observed gas-liquid demixing with increasing dextran concentration using turbidity measurement. The solutions with varying polymer concentrations were prepared at pH = 6.4 in the presence of $c_{\rm s} = 0.5\,{\rm mol/l}$ NaCl. At this pH globulin is assumed to carry $Z = 25$ negative charges [75]. Its mass density is $1.351\,{\rm g/cm^3}$ [76] and it has a Stokes radius of $a = (5.7 \pm 0.3)$ nm [76] and a molar mass of 150 kg/mol [74]. At room temperature ($T = 25\,^\circ{\rm C}$), the Bjerrum length is $l_{\rm B} = 0.71\,{\rm nm}$. Now

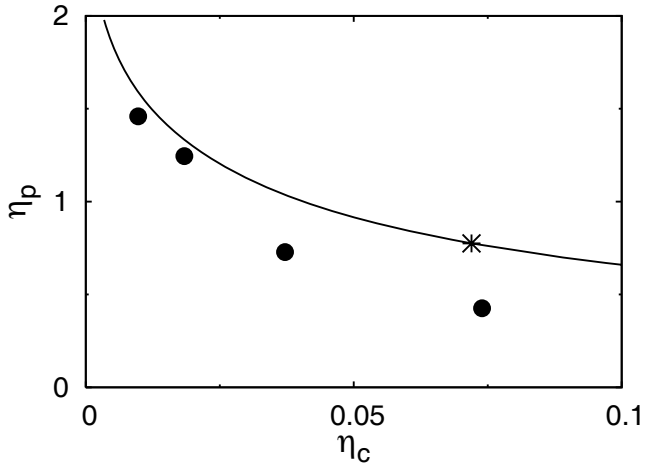

Fig. 15. Phase diagram of a mixture of globulin and dextran at pH = 6.4 in 0.5 mol/l NaCl. The data points are redrawn from Hoskins *et al.* [74]. The solid curve is the theoretically predicted binodal obtained using GFVT for weakly charged spheres plus interacting polymers for $q = 2.3$ and $m = 1.02$, assuming θ-solvent conditions. The asterisk marks the critical point calculated from GFVT.

we have $\beta\epsilon = 0.19$ as contact potential, and $\kappa a = 13.3$ as Debye screening parameter, where we assumed $\rho_c = 0$ in equation (2). Then, from equation (4) and equation (3) we obtain $m = 1.020$. Thus, our model calculations are applicable here. We note that m always decreases with increasing η_c within the DLVO approximation due to the contribution to the electrostatic screening by the surface released counter-ions (see Eq. (2)). It follows that the condition on m is also fulfilled for all non-zero protein volume fractions η_c. For example, one obtains $m = 1.018$ at $\eta_c = 0.4$ and $c_s = 0.5$ mol/l ($\beta\epsilon = 0.18$ and $\kappa a = 13.8$). However, we will neglect the (colloidal) density dependence of κ in the following for simplicity. Therefore, we use $m = 1.020$. Hoskins *et al.* [74] used dextran with a molar mass of $M_w = 267$ kg/mol and a radius of gyration of $R_g = 13$ nm [77]. Hence, we use $q = 2.3$. In Figure 15 we compare the experimentally observed phase diagram of Hoskins *et al.* [74] with ours from GFVT theoretically predicted binodal assuming θ-solvent conditions. The theoretically predicted gas-liquid coexistence curve overestimates the polymer concentration at which phase separation sets in slightly with increasing η_c. The deviation of the theoretically predicted binodal from the experimental data points might be due to the branched structure of dextran [77] and presumably due to the polydispersity in R_g leading to an underestimation of the osmotic pressure and, thus, shifting the calculated gas-liquid coexistence curve to larger polymer concentrations. Nevertheless, the theoretical and experimental binodals agree well especially if one takes into account that no adjustable parameters have been used.

5 Conclusion

We have investigated the influence of additional, charge-induced repulsions between the colloids and the effect of interacting polymers in good and θ-solvent conditions on the phase behaviour of colloid-polymer mixtures. This has been accomplished by incorporating colloidal electrostatic repulsions into a recently formulated generalised free-volume theory. First, we have demonstrated that the proposed theory is in quantitative agreement with previously performed Monte Carlo computer simulation results for uncharged colloids in case of polymer-to-colloid size ratios smaller than unity and in overall good semi-quantitative agreement for size ratios above unity. Secondly, in case of charged colloidal particles, we find a strong influence of the range of repulsion on the phase stability of mixtures of polymer chains and charged spheres. The charge-induced repulsions between the colloids stabilise colloid-polymer mixtures against gas-liquid phase separation. In addition, the crystallisation curve shifts to lower colloid volume fractions with increasing repulsion. Thirdly, we find that the solvent for the polymers in solution further affects the phase diagram significantly. The stability region, where a stable fluid is found, is larger for a good solvent compared to a θ-solvent; the influence of the solvency is larger for larger polymer-to-colloid size ratio. This is due to the fact that phase separation takes place at larger polymer concentrations (when normalised with the polymer overlap concentration). Finally, we find good agreement when comparing our theoretically predicted and experimentally observed binodal in an aqueous mixture of charged globulin (protein) and dextran (polysaccharide). From our work it follows that it is useful for experimentalists working on biological systems such as protein/polysaccharide mixtures to characterise the solvent quality of the biopolymers in solution. Then it is easier to make predictions for the phase stability.

We thank A.-P. Hynninen and P.G. Bolhuis for providing us with MC simulation data.

References

1. W.B. Russel, D.A. Saville, W.R. Schowalter, *Colloidal Dispersions* (Cambridge University Press, Cambridge, 1992).
2. W.C.K. Poon, J. Phys.: Condens. Matter **14**, R859 (2002).
3. R. Tuinier, J. Rieger, C.G. de Kruif, Adv. Colloid Interface Sci. **103**, 1 (2003).
4. S. Asakura, F. Oosawa, J. Chem. Phys. **22**, 1255 (1954).
5. S. Asakura, F. Oosawa, J. Polym. Sci. **33**, 183 (1958).
6. A. Vrij, Pure Appl. Chem. **48**, 471 (1976).
7. A.P. Gast, C.K. Hall, W.B. Russel, J. Colloid Interface Sci. **96**, 251 (1983).
8. H. de Hek, A. Vrij, J. Colloid Interface Sci. **84**, 409 (1981).
9. B. Vincent, Colloids Surf. **24**, 269 (1987).
10. B. Vincent, J. Edwards, S. Emmett, R. Croot, Colloids Surf. **31**, 267 (1988).
11. H.N.W. Lekkerkerker, W.C.K. Poon, P.N. Pusey, A. Stroobants, P.W. Warren, Europhys. Lett. **20**, 559 (1992).
12. H.L. Reiss, H. Frisch, J.L. Lebowitz, J. Chem. Phys. **31**, 369 (1959).
13. J.L. Lebowitz, E. Helfand, E. Praestgaard, J. Chem. Phys. **43**, 774 (1965).

14. E.J. Meijer, D. Frenkel, J. Chem. Phys. **100**, 6873 (1994).
15. R.C.L. Vink, J. Horbach, J. Chem. Phys. **121**, 3253 (2004).
16. M. Dijkstra, J.M. Brader, R. Evans, J. Phys.: Condens. Matter **11**, 10079 (1999).
17. M. Dijkstra, R. van Roij, R. Evans, Phys. Rev. E **59**, 5744 (1999).
18. M. Dijkstra, R. van Roij, R. Evans, Phys. Rev. Lett. **82**, 117 (1999).
19. M. Dijkstra, R. van Roij, R. Evans, J. Chem. Phys. **113**, 4799 (2000).
20. M. Dijkstra, R. van Roij, R. Roth, A. Fortini, Phys. Rev. E **73**, 041404 (2006).
21. A. Moncho-Jordá, A.A. Louis, P.G. Bolhuis, R. Roth, J. Phys.: Condens. Matter **15**, S3429 (2003).
22. M. Fuchs, K.S. Schweizer, J. Chem. Phys. **106**, 347 (1997).
23. M. Fuchs, K.S. Schweizer, Europhys. Lett. **51**, 621 (2000).
24. M. Fuchs, K.S. Schweizer, Phys. Rev. E **64**, 021514 (2001).
25. Y.L. Chen, K.S. Schweizer, J. Chem. Phys. **118**, 3880 (2003).
26. M. Fuchs, K.S. Schweizer, J. Phys.: Condens. Matter **14**, R239 (2002).
27. S. Ramakrishnan, M. Fuchs, K.S. Schweizer, C.F. Zukoski, Langmuir **18**, 1082 (2002).
28. S. Ramakrishnan, M. Fuchs, K.S. Schweizer, C.F. Zukoski, J. Chem. Phys. **116**, 2201 (2002).
29. S.A. Shah, S. Ramakrishnan, Y.L. Chen, K.S. Schweizer, C.F. Zukoski, Langmuir **19**, 5128 (2003).
30. C.P. Royall, D.G.A.L. Aarts, H. Tanaka, Nat. Phys. **3**, 636 (2007).
31. D. Pini, F. Lo Verso, M. Tau, A. Parola, L. Reatto, Phys. Rev. Lett. **100**, 055703 (2008).
32. V.B. Tolstoguzov, Food Hydrocolloids **4**, 429 (1991).
33. V. Ya Grinberg, V.B. Tolstoguzov, Food Hydrocolloids **11**, 145 (1997).
34. D. Marenduzzo, K. Finan, P.R. Cook, J. Cell. Biol. **175**, 681 (2006).
35. T. Odijk, Biophys. J. **73**, 23 (1988).
36. R. de Vries, Biophys. J. **80**, 1186 (2001).
37. A. McPherson, *Crystallization of Biological Macromolecules*, 1st edition (Cold Spring Harbor Laboratory Press, New York, 1999).
38. P.G. Bolhuis, A.A. Louis, Macromolecules **35**, 1860 (2002).
39. P.G. Bolhuis, A.A. Louis, J.P. Hansen, E.J. Meijer, J. Chem. Phys. **114**, 4296 (2001).
40. A.A. Louis, P.G. Bolhuis, J.P. Hansen, E.J. Meijer, Phys. Rev. Lett. **85**, 2522 (2000).
41. P.G. Bolhuis, A.A. Louis, J.P. Hansen, Phys. Rev. Lett. **89**, 128302 (2002).
42. M. Schmidt, M. Fuchs, J. Chem. Phys. **117**, 6308 (2002).
43. D.G.A.L. Aarts, R. Tuinier, H.N.W. Lekkerkerker, J. Phys.: Condens. Matter **14**, 7551 (2002).
44. E. Eisenriegler, A. Hanke, S. Dietrich, Phys. Rev. E **54**, 1134 (1996).
45. A. Hanke, E. Eisenriegler, S. Dietrich, Phys. Rev. E **59**, 6853 (1999).
46. F.W. Tavares, S.I. Sandler, AIChE J. **43**, 218 (1997).
47. P.G. Ferreira, M. Dymitrowska, L. Belloni, J. Chem. Phys. **113**, 9849 (2000).
48. Ferreira and Belloni have chosen a system of highly charged and weakly screened colloids and non-adsorbing polymer chains ($a = 10\,\mathrm{nm}$, $R_\mathrm{g} = 10\,\mathrm{nm}$, $Z = 50$, $c_\mathrm{s} = 0.01\,\mathrm{mol/l}$, $T = 298\,\mathrm{K}$). These values lead to a factor of $m = 7.5$, and, thus, cannot be described by our simple model because the Coulomb interactions are no longer short ranged with respect to the colloid size. Therefore, we cannot compare with their calculated gas-liquid spinodal for $Z = 0$ and $Z = 50$ (see Fig. 11 on page 9860 in [47]).
49. A.R. Denton, M. Schmidt, J. Chem. Phys. **122**, 244911 (2005).
50. A. Fortini, M. Dijkstra, R. Tuinier, J. Phys.: Condens. Matter **17**, 7783 (2005).
51. G.J. Fleer, R. Tuinier, Phys. Rev. E **76**, 041802 (2007).
52. G.J. Fleer, A.M. Skvortsov, R. Tuinier, Macromol. Theory Simul. **16**, 531 (2007).
53. R. Tuinier, P.A. Smith, W.C.K. Poon, S.U. Egelhaaf, D.G.A.L. Aarts, H.N.W. Lekkerkerker, G.J. Fleer, Europhys. Lett. **82**, 68002 (2008).
54. J.A. Barker, D. Henderson, J. Chem. Phys. **47**, 4714 (1967).
55. H.N.W. Lekkerkerker, Colloids Surf. **51**, 419 (1990).
56. S.M. Oversteegen, R. Roth, J. Chem. Phys. **122**, 214502 (2005).
57. J.M. Brader, M. Dijkstra, R. Evans, Phys. Rev. E **63**, 041405 (2001).
58. A.A. Louis, P.G. Bolhuis, E.J. Meijer, J.P. Hansen, J. Chem. Phys. **117**, 1893 (2002).
59. N.F. Carnahan, K.E. Starling, J. Chem. Phys. **51**, 635 (1969).
60. W.W. Wood, J. Chem. Phys. **20**, 1334 (1952).
61. D. Frenkel, A.J.C. Ladd, J. Chem. Phys. **81**, 3188 (1984).
62. G.J. Fleer, R. Tuinier, Physica A **379**, 52 (2007).
63. E. Eisenriegler, J. Chem. Phys. **79**, 1052 (1983).
64. P.G. de Gennes, *Scaling Concepts in Polymer Physics* (Cornell University Press, Ithaca, 1979).
65. G.J. Fleer, A.M. Skvortsov, R. Tuinier, Macromolecules **36**, 7857 (2003).
66. A.A. Louis, P.G. Bolhuis, E.J. Meijer, J.P. Hansen, J. Chem. Phys. **116**, 10547 (2002).
67. T. Taniguchi, T. Kawakatsu, K. Kawasaki, *Slow Dynamics in Condensed Matter*, AIP Conf. Ser., Vol. **256** (American Institute of Physics, New York, 1992) p. 503.
68. G.J. Fleer, R. Tuinier, in press, Adv. Colloid Interface Sci. (2008) doi: 10.1016/j.cis.2008.07.001, 2008.
69. P.G. Bolhuis, E.J. Meijer, A.A. Louis, Phys. Rev. Lett. **90**, 068304 (2003).
70. W.G. Hoover, F.H. Ree, J. Chem. Phys. **49**, 3609 (1968).
71. A.P. Hynninen, M. Dijkstra, Phys. Rev. E **68**, 021407 (2003).
72. A.A. Louis, J. Phys.: Condens. Matter **14**, 9187 (2002).
73. D. Frenkel, Physica A **313**, 1 (2002).
74. A.R. Hoskins, I.D. Robb, P.A. Williams, Biopolymers **45**, 97 (1998).
75. C.L.A. Berli, J.A. Deiber, M.C. Anon, Food Hydrocolloids **13**, 507 (1999).
76. H. Chick, C.J. Martin, Biochem. J. **7**, 92 (1913).
77. E. Nordmeier, J. Phys. Chem. **97**, 5770 (1993).